Deconfinement and chiral phase transitions in quark matter with a strong electric field

William R. Tavares,[1,*] Ricardo L. S. Farias,[2,†] and Sidney S. Avancini[1,‡]

[1]*Departamento de Física, Universidade Federal de Santa Catarina, 88040-900 Florianópolis, Santa Catarina, Brazil*

[2]*Departamento de Física, Universidade Federal de Santa Maria, 97105-900 Santa Maria, Rio Grande do Sul, Brazil*

(Received 4 December 2019; published 29 January 2020)

The deconfinement and chiral phase transitions are studied in the context of the electrized quark matter at finite temperature in the two-flavor Polyakov–Nambu–Jona-Lasinio model. Using the mean field approximation and an electric field independent regularization we show that the effect of temperature and/or electric fields is to partially restore the chiral symmetry. The deconfinement phase transition is slightly affected by the magnitude of the electric field. To this end we show how the effective quark masses and the expectation value of the Polyakov loop are affected by the electric fields at finite temperatures. As a very interesting result, the pseudocritical temperatures for chiral symmetry restoration and deconfinement decrease as we increase the magnitude of the electric fields; however, both start to increase after some critical value of the electric field.

DOI: 10.1103/PhysRevD.101.016017

I. INTRODUCTION

Recent numerical simulations provide possibilities for strong electromagnetic fields to be present in noncentral heavy ion collisions (HIC) [1–4]. These indications suggest even more properties to be explored in the strongly interacting quark matter, besides the usual strong magnetic fields [5], that are supposed to be created in noncentral HIC or in magnetars [6,7]. The event-by-event fluctuations of the proton positions in the colliding nuclei in $\mathrm{Au}+\mathrm{Au}$ heavy-ion collisions at $\sqrt{s}=200$ GeV in RHIC@BNL and $\mathrm{Pb}+\mathrm{Pb}$ at $\sqrt{s}=2.76$ TeV in ALICE@LHC indicate the creation of strong electric fields that can be of the same order of magnitude of the already predicted magnetic fields [1–3,8]. In asymmetric $\mathrm{Cu}+\mathrm{Au}$ collisions [4,9,10] it is expected that a strong electric field is generated in the overlapping region. This happens because there is a different number of electric charges in each nuclei and it is argued that this is a fundamental property due to the charge dipole formed in the early stage of the collision. Also, different projectile-target combinations are studied from symmetric to asymmetric collisions systems, showing that the electric field is more significant in the former [11]. The time evolution for electric and magnetic fields in HIC can be estimated and the prediction depends on the conductivity of the medium [12]. In a complementary way, the study of strong electric fields can be very useful when searching for the chiral magnetic effect (CME) [5], given the speculated possibility of reversing the sign of some experimental observables related to the CME [4,13] if the lifetime of such fields is long enough. Such scenarios could give an opportunity to explore anomalous transport properties such as chiral electric separation [14–17], which is a generation of an axial current in a system with both vector and axial densities [18].

It is natural in this scenario to ask how some properties of quantum chromodynamics(QCD) under strong conditions (i.e., high temperatures and densities) can be affected by such fields. In the low energy limit we should use effective theories or lattice QCD (LQCD) techniques, once we are dealing with the nonperturbative behavior of QCD. One of the main aspects that should be explored is the chiral symmetry restoration of QCD, where several studies have explored a series of interesting phenomena, like the magnetic catalysis [19–21], the chiral magnetic effect [5], and the inverse magnetic catalysis [22–27] predicted by lattice QCD results [28,29], all of them studied in the context of a pure magnetic field. A natural extension of these works can be done by exploring the role of magnetic fields in the deconfinement transition as well [30–35]. The effective theories or LQCD investigations in general are dealing with

*william.tavares@posgrad.ufsc.br
†ricardo.farias@ufsm.br
‡sidney.avancini@ufsc.br

the chiral condensate, which is an approximate order parameter for the chiral phase transition [30]. On the other hand, the deconfinement in a gauge theory is associated with the spontaneous symmetry breaking of the center symmetry, in which the approximate order parameter is the Polyakov loop [36,37]. The predictions of some effective models for the physics associated with the Polyakov loop have been widely studied in the literature [38–42].

The main goal of our work is to include for the first time the effects of a pure electric field on the Polyakov extended SU(2) Nambu–Jona-Lasinio model (PNJL) [43], to study how the deconfinement phase transition temperature T^l_{pc} is affected by these fields, and also to explore its connection with the chiral pseudocritical temperature T^χ_{pc}. To this end, we will implement the Schwinger proper-time quark propagators in a constant electric field, which have been explored in previous works [44–47] related to the study of the gap equation and thermodynamical properties of the model. We also implement in the Schwinger proper-time formalism the Polyakov loop, which should be useful for future evaluations even at $eE = 0$. As the Nambu–Jona-Lasinio model SU(2) model (NJL) in $3+1$ D is non-renormalizable, the regularization procedure is the same as that presented in [44], where the pure-electric field contribution was analytically solved and the finite thermoelectric part was numerically evaluated. Finally, the Schwinger pair production [48,49] will be presented. Previous studies have shown [44,45] that in the present approximation this quantity is mainly determined by the effective quark masses, which in turn incorporates the effects of temperature and electric field. Thus, there will be quantitative differences between the results for the pair production rate when calculated in the PNJL or NJL model.

The work is organized as follows. In Sec. II we introduce the standard formalism for the two-flavor NJL and PNJL models at finite temperature, including the effects due to the strong electric field. In Sec. III we present the regularization scheme adopted in this work. In Sec. IV we present our numerical results. Finally, in Sec. V we discuss our results and conclusions. We leave for the Appendix the explicit calculations of the trace of the Polyakov loop.

II. GENERAL FORMALISM

In the presence of an electromagnetic field the two-flavor NJL model Lagrangian can be written as

$$\mathcal{L} = \bar{\psi}(i\not{D} - \tilde{m})\psi + G[(\bar{\psi}\psi)^2 + (\bar{\psi}i\gamma_5\vec{\tau}\psi)^2] - \frac{1}{4}F^{\mu\nu}F_{\mu\nu}, \tag{1}$$

where A^μ, $F^{\mu\nu} = \partial^\mu A^\nu - \partial^\nu A^\mu$ are the electromagnetic gauge potential and tensor fields, respectively; G is the coupling constant; and $D^\mu = (i\partial^\mu - QA^\mu)$ is the covariant derivative.

Also, $\vec{\tau}$ are the isospin Pauli matrices; Q is the diagonal quark charge matrix, $\mathrm{Q} = \mathrm{diag}(q_u = 2e/3, q_d = -e/3)$; $\psi = (\psi_u, \psi_d)^T$ is the two-flavor quark fermion field; and $\tilde{m} = \mathrm{diag}(m_u, m_d)$ represents the current quark mass matrix. Here, we adopt the isospin approximation, i.e., $m_u = m_d = m$. We choose $A_\mu = -\delta_{\mu 0}x_3 E$ in order to obtain a constant electric field in the z-direction.

In the mean field approximation the Lagrangian density reads

$$\mathcal{L} = \bar{\psi}(i\not{D} - M)\psi + G\langle\bar{\psi}\psi\rangle^2 - \frac{1}{4}F^{\mu\nu}F_{\mu\nu}, \tag{2}$$

where the constituent quark mass is defined by the following expression:

$$M = m - 2G\sum_{f=u,d}(\phi_f^{\mathcal{E}} + \phi_f^{\mathcal{E},T}), \tag{3}$$

where we have both a pure electric field, $\phi_f^{\mathcal{E}}$, and a thermoelectric field, $\phi_f^{\mathcal{E},T}$, contribution. We will use the following definition of the quark condensate:

$$\phi_f = \langle\bar{\psi}_f\psi_f\rangle = -\int\frac{d^4p}{(2\pi)^4}\mathrm{Tr}[iS_f(p)], \tag{4}$$

where $f = u, d$ stands for the quark flavors. Following the procedure described in [44], the pure electric condensate contribution $\phi_f^{\mathcal{E}}$ can be calculated using the full Schwinger proper-time quark propagator [48] in a constant electric field, resulting in the expression

$$\phi_f^{\mathcal{E}} = -\frac{MN_c}{4\pi^2}\mathcal{E}_f\int_0^\infty ds\frac{e^{-sM_f^2}}{s}\cot(\mathcal{E}_f s), \tag{5}$$

where $\mathcal{E}_f = |q_f|E$ and $N_c = 3$ is the number of colors.

As already derived in [44,45], the thermoelectric contribution can be written as

$$\phi_f^{\mathcal{E},T} = -\frac{MN_c}{2\pi^2}\sum_{n=1}^\infty(-1)^n\mathcal{E}_f\int_0^\infty ds\frac{e^{-sM_f^2}}{s}\cot(\mathcal{E}_f s) \times e^{-\frac{\mathcal{E}_f n^2}{4|\tan(\mathcal{E}_f s)|T^2}}. \tag{6}$$

The thermodynamical potential has been derived in [44,45] simply by integrating Eq. (3) with respect to the effective quark mass M, yielding

$$\Omega = \frac{(M-m)^2}{4G} - \sum_{f=u,d}(\theta_f^{\mathcal{E}} + \theta_f^{\mathcal{E},T}), \tag{7}$$

where we have defined $\theta_f^{\mathcal{E}}$ and $\theta_f^{\mathcal{E},T}$ as

$$\theta_f^{\mathcal{E}} = -\frac{N_c}{8\pi^2}\int_0^\infty ds\frac{e^{-sM^2}}{s^2}\mathcal{E}_f\cot(\mathcal{E}_f s), \tag{8}$$

$$\theta_f^{\mathcal{E},T} = -\frac{N_c}{4\pi^2}\sum_{n=1}^{\infty}(-1)^n\int_0^\infty ds\frac{e^{-sM^2}}{s^2}\mathcal{E}_f\cot(\mathcal{E}_f s) \times e^{-\frac{\mathcal{E}_f n^2}{4|\tan(\mathcal{E}_f s)|T^2}}. \quad (9)$$

The Schwinger pair production rate is given by $\Gamma = -2\Im(\Omega)$ [45,48], where $\Im(\Omega)$ corresponds to the imaginary part of the effective potential. Explicitly, one obtains for Γ

$$\Gamma(M,\mathcal{E},T) = \frac{N_c}{4\pi}\sum_f \mathcal{E}_f^2\sum_{k=1}^{\infty}\frac{e^{-\frac{M^2\pi k}{\mathcal{E}_f}}}{(k\pi)^2}, \quad (10)$$

where we need to perform the summation over the flavor indices $f = u$, d, and as we will see later, the entire Schwinger pair production dependence on the external conditions is contained only in the effective mass $M \equiv M(\mathcal{E},T)$.

A. The electrized SU(2) PNJL

The extended version of the two-flavor NJL model Lagrangian in the presence of an electromagnetic field coupled with the Polyakov loop is given by

$$\mathcal{L} = \bar{\psi}(i\not{D} - \tilde{m})\psi + G[(\bar{\psi}\psi)^2 + (\bar{\psi}i\gamma_5\vec{\tau}\psi)^2] - \frac{1}{4}F^{\mu\nu}F_{\mu\nu} - \mathcal{U}(l,\bar{l},T); \quad (11)$$

now the covariant derivative is given by $D^\mu = (i\partial^\mu - QA^\mu - i\mathcal{A}^\mu)$, where $\mathcal{A}^\mu = \delta_0^\mu\mathcal{A}^0$ is the Polyakov gauge, the strong coupling constant g is absorbed in the definition $\mathcal{A}^\mu(x) = g\frac{\lambda_a}{2}\mathcal{A}_a^\mu(x)$, λ_a are the Gell-Mann matrices, and $\mathcal{A}_a^\mu(x)$ is the SU(3) gauge field.

For the pure gauge sector, let us define the Polyakov line as

$$L(x) = \mathcal{P}\exp\left[i\int_0^\beta d\tau\mathcal{A}_4(\tau,\vec{x})\right], \quad (12)$$

where $\mathcal{P}$ is a path ordering and $\beta = \frac{1}{T}$. Also, $\mathcal{A}_4 = i\mathcal{A}_0$ is the temporal component of the Euclidean gauge field $(\mathcal{A}_4,\vec{\mathcal{A}})$.

The effective potential $\mathcal{U}(l,\bar{l},T)$ for the Polyakov fields is parametrized in order to reproduce lattice results in the mean field approximation [38,39]. We adopt the *Ansatz* [39],

$$\frac{\mathcal{U}(l,\bar{l},T)}{T^4} = -\frac{b_2(T)l\bar{l}}{2} - \frac{b_3(l^3+\bar{l}^3)}{6} + \frac{b_4(l\bar{l})^2}{4}, \quad (13)$$

where $b_2(T)$ is given by

$$b_2(T) = a_0 + a_1\left(\frac{T_0}{T}\right) + a_2\left(\frac{T_0}{T}\right)^2 + a_3\left(\frac{T_0}{T}\right)^3. \quad (14)$$

The parameters of the potential $\mathcal{U}(l,\bar{l},T)$ will be given in Sec. IV. We should also mention that the thermal expectation value of the Polyakov loop is given by [40]

$$l \equiv \frac{1}{N_c}\langle\mathrm{Tr}_c L(x)\rangle, \qquad \bar{l} \equiv \frac{1}{N_c}\langle\mathrm{Tr}_c L^\dagger(x)\rangle. \quad (15)$$

As we will see, our most interesting results occur for temperatures around the pseudocritical temperatures for deconfinement T_{pc}^l and for chiral symmetry restoration T_{pc}^χ. We verify that the different *Ansätze* for $U(l,\bar{l},T)$ [50] almost agree in this region. Therefore, our results remain essentially the same if we change the form of the effective potential for the Polyakov loop $U(l,\bar{l},T)$.

Once we are working with the background field $\mathcal{A}_4$, we can obtain the condensate as a straightforward generalization of the expression given in Eq. (4) for zero temperature and density using the following symbolic replacements [41]:

$$i\int\frac{d^4p}{(2\pi)^4} \to -T\frac{1}{N_c}\mathrm{Tr}_c\sum_{n=-\infty}^{\infty}\int\frac{d^3p}{(2\pi)^3}, \quad (16)$$

$$(p_0,\vec{p}) \to (i\omega_n + \mu - i\mathcal{A}_4,\vec{p}), \quad (17)$$

where $w_n = (2n+1)\pi T$ is the Matsubara frequency. In this work we consider only the zero baryon chemical potential case, and hence $l = \bar{l}$. Once the traced Polyakov loop is given by $l = \frac{1}{N_c}\mathrm{Tr}\exp(i\frac{\mathcal{A}_4}{T})$, we can write the background field in the Polyakov gauge [42,51] as $\mathcal{A}_4 = g\mathcal{A}_4^{(3)}\frac{\lambda_3}{2} + g\mathcal{A}_4^{(8)}\frac{\lambda_8}{2}$, and it is straightforward to see that $\mathcal{A}_4^{(8)} = 0$ at $\mu = 0$. Therefore, we implement the Polyakov loop in the condensate $\phi^{\mathcal{E},T,l}$ at $\mu = 0$ by using the prescriptions given by Eqs. (16) and (17). After calculating the trace in the color space, one obtains

$$\phi_f^{\mathcal{E},T,l} = -\frac{M}{2\pi^2}\sum_{n=1}^{\infty}(-1)^n\mathcal{E}_f\int_0^\infty ds\frac{e^{-sM^2}}{s}\cot(\mathcal{E}_f s) \times e^{-\frac{\mathcal{E}_f n^2}{4|\tan(\mathcal{E}_f s)|T^2}}\left\{1 + 2\cos\left[n\cos^{-1}\left(\frac{3l-1}{2}\right)\right]\right\}. \quad (18)$$

By making use of this expression in Eq. (3) the SU(2) PNJL gap equation reads

$$\frac{M-m}{2G} = -\sum_{f=u,d}(\phi_f^{\mathcal{E}} + \phi_f^{\mathcal{E},T,l}). \quad (19)$$

Finally, the thermodynamical or effective potential is obtained following a standard procedure [41] using the prescriptions (16) and (17), yielding

$$\Omega = \mathcal{U}(l,T) + \frac{(M-m)^2}{4G} - \sum_{f=u,d}(\theta_f^{\mathcal{E}} + \theta_f^{\mathcal{E},T,l}). \quad (20)$$

It is straightforward to show that

$$\theta_f^{\mathcal{E}} = -\frac{N_c}{8\pi^2}\int_0^\infty ds\frac{e^{-sM^2}}{s^2}\mathcal{E}_f\cot(\mathcal{E}_f s), \quad (21)$$

$$\theta_f^{\mathcal{E},T,l} = -\frac{1}{4\pi^2}\sum_{n=1}^{\infty}(-1)^n \int_0^\infty ds \frac{e^{-sM^2}}{s^2}\mathcal{E}_f \cot(\mathcal{E}_f s) \times e^{-\frac{\mathcal{E}_f n^2}{4|\tan(\mathcal{E}_f s)|T^2}}\left\{1+2\cos\left[n\cos^{-1}\left(\frac{3l-1}{2}\right)\right]\right\}. \tag{22}$$

The effective quark masses and the expectation value of the Polyakov loop are obtained by minimizing the thermodynamical potential, i.e., calculating $\frac{\partial\Omega}{\partial M}=0$ and $\frac{\partial\Omega}{\partial l}=0$. The derivative $\frac{\partial\Omega}{\partial M}=0$ was already obtained in Eq. (19) and $\frac{\partial\Omega}{\partial l}=0$ is given by

$$0 = \frac{T^4}{2}[-b_2(T)l - b_3 l^2 + b_4 l^3] + \frac{1}{4\pi^2}\sum_{f=u,d}\int_0^\infty \frac{ds}{s^2}e^{-sM^2}\mathcal{E}_f\cot(\mathcal{E}_f s)\sum_{n=0}^{\infty}(-1)^n \times e^{-\frac{\mathcal{E}_f n^2}{4|\tan(\mathcal{E}_f s)|T^2}}\left\{\frac{\sqrt{3}n\sin[n\cos^{-1}(\frac{3l-1}{2})]}{\sqrt{-3l^2+2l+1}}\right\}. \tag{23}$$

III. REGULARIZATION

In this work we use the vacuum-subtraction scheme [44–47]. We define for the vacuum-subtracted condensate the following quantity:

$$\bar{\phi}_f^{\mathcal{E}} = -\frac{MN_c}{4\pi^2}\int_0^\infty ds\frac{e^{-sM^2}}{s^2}[\mathcal{E}_f s\cot(\mathcal{E}_f s)-1]. \tag{24}$$

The gap equation, Eq. (3) in the SU(2) NJL model and Eq. (19) in the SU(2) PNJL, should be calculated using the following regularized condensate $\phi_f^{\mathcal{E}}$:

$$\phi_f^{\mathcal{E}} = \bar{\phi}_f^{\mathcal{E}} + \phi_f^{\text{vac}}, \tag{25}$$

where we have adopted the 3D cutoff scheme [52,53] to regularize the infinite field independent vacuum contribution

$$\phi_f^{\text{vac}} = -\frac{MN_c}{2\pi^2}\left[\Lambda\mathcal{E}_\Lambda - M^2\ln\left(\frac{\mathcal{E}_\Lambda+\Lambda}{M}\right)\right], \tag{26}$$

where $\mathcal{E}_\Lambda = \sqrt{\Lambda^2+M_f^2}$. In the same way, for the effective potential in the SU(2) NJL model, Eq. (7), and Eq. (20) in the SU(2) PNJL model, we should use the regularized $\theta_f^{\mathcal{E}}$ given by

$$\theta_f^{\mathcal{E}} = \bar{\theta}_f^{\mathcal{E}} + \theta_f^{\text{vac}}, \tag{27}$$

where the finite field dependent term is

$$\bar{\theta}_f^{\mathcal{E}} = -\frac{N_c}{8\pi^2}\int_0^\infty ds\frac{e^{-sM^2}}{s^3}\left[\mathcal{E}_f s\cot(\mathcal{E}_f s) - 1 + \frac{(\mathcal{E}_f s)^2}{3}\right], \tag{28}$$

and the infinite vacuum contribution θ_f^{vac} is given by

$$\theta_f^{\text{vac}} = \frac{N_c}{8\pi^2}\int_0^\infty ds\frac{e^{-sM^2}}{s^3}. \tag{29}$$

The regularized θ_f^{vac} is given in the 3D cutoff scheme by

$$\theta_f^{\text{vac}} = -\frac{N_c}{8\pi^2}\left[M^4\ln\left(\frac{\Lambda+\sqrt{\Lambda^2+M^2}}{M}\right) - \Lambda\sqrt{\Lambda^2+M^2}(M^2+2\Lambda^2)\right]. \tag{30}$$

It is important to note that the poles associated with the imaginary part of the effective potential can be associated to the zeros of the $\sin(\mathcal{E}_f s)$ which appear in the denominator of both our gap equation and the effective potential when $\mathcal{E}_f s = n\pi$ for $n = 1, 2, 3, \ldots$. We interpret these integrals as the Cauchy principal value [44,46] and that the true ground state of the theory is given by the real part of the thermodynamical potential.

Using the techniques adopted in [44], we can use the principal value (or the real part) of $\bar{\theta}_f^{\mathcal{E}}$, given by

$$\Re(\bar{\theta}_f^{\mathcal{E}}) = -\frac{N_c}{2\pi^2}(\mathcal{E}_f)^2\left\{\zeta'(-1) + \frac{\pi}{4}y_f + \frac{y_f^2}{2}\left(\gamma_E - \frac{3}{2} + \ln y_f\right) - \frac{1}{12}(1+\ln y_f) + \sum_{k=1}^{\infty}k\left[\frac{y_f}{k}\tan^{-1}\left(\frac{y_f}{k}\right) - \frac{1}{2}\ln\left(1+\left(\frac{y_f}{k}\right)^2\right) - \frac{1}{2}\left(\frac{y_f}{k}\right)^2\right]\right\}, \tag{31}$$

where $y_f = M^2/(2\mathcal{E}_f)$. In the same manner, we obtain for the principal value of the vacuum-subtracted condensate $\bar{\phi}_f^{\mathcal{E}}$

$$\Re(\bar{\phi}_f^{\mathcal{E}}) = -\frac{MN_c}{4\pi^2}\int_0^\infty ds\frac{e^{-sM^2}}{s^2}[\mathcal{E}_f s\cot(\mathcal{E}_f s)-1] = \frac{MN_c}{2\pi^2}\mathcal{E}_f\left[\frac{\pi}{4} + y_f(\gamma_E - 1 + \ln y_f) + \sum_{k=1}^{\infty}\left(\tan^{-1}\frac{y_f}{k} - \frac{y_f}{k}\right)\right]. \tag{32}$$

As discussed in [44], the quantities $\phi_f^{\mathcal{E},T}$ and $\theta_f^{\mathcal{E},T}$ depend on the temperature and following the procedure adopted in Ref. [54] we set the lower limits of the integration to zero, since theses integrals are ultraviolet finite.

IV. NUMERICAL RESULTS

In this section we show our numerical results. The parameter set for the SU(2) NJL model is [53] $\Lambda = 587.9$ MeV, $G\Lambda^2 = 2.44$, and $m = 5.6$ MeV. The

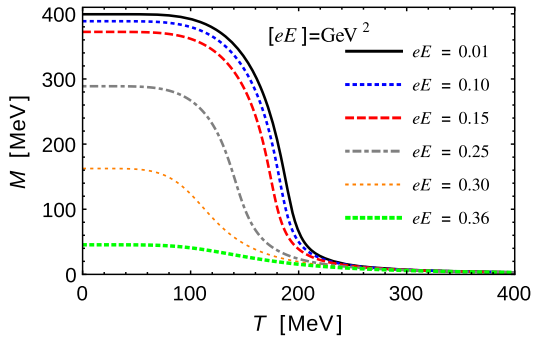

FIG. 1. Constituent quark mass M as a function of the temperature for different values of eE in the SU(2) NJL model.

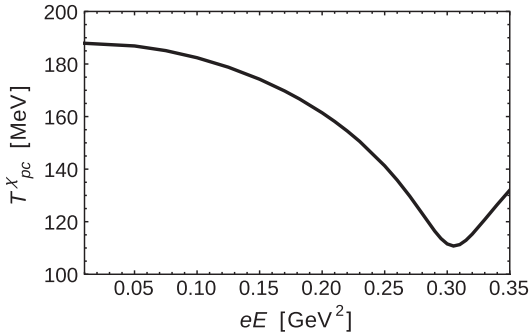

FIG. 3. Pseudocritical temperature for chiral symmetry restoration T^{χ}_{pc} as a function of eE in the SU(2) NJL model.

parameters associated with the pure gauge sector are the following: $a_0 = 6.75$, $a_1 = -1.95$, $a_2 = 2.625$, $a_3 = -7.44$, $b_3 = 0.75$, and $b_4 = 7.5$. In the pure gauge sector, the transition temperature is given by $T_0 = 270$ MeV [39]. A lower value of T_0 is usually necessary in order to include the effects of $N_f = 2$ in the theory. Following the procedure adopted in Refs. [35,55], we use $T_0 = 208$ MeV.

In Fig. 1 we show the effective quark masses as a function of the temperature for different values of electric fields in the two-flavor NJL model. As expected, for the NJL model at $eE = 0.01$ GeV^2, as we increase the temperature, the effective quark masses decrease, as a signature of the chiral symmetry restoration. If we increase the electric field to $eE = 0.10$ GeV^2, at low temperatures the effective quark masses slightly decrease as an effect of the restoration of the chiral symmetry guided by the electric field. This effect was already explored in previous works in the literature at finite temperature [44,45] and at $T = 0$ [52,56]. As we increase the electric field it can be seen that the pseudocritical temperature has decreased with the increase of the electric field. In Fig. 2, we show how $-\frac{dM}{dT}$ changes with the increase of the electric field. The peak of each curve is interpreted as the pseudocritical temperature for chiral symmetry restoration T^{χ}_{pc} for the corresponding electric field. In Fig. 3 we can see the pseudocritical temperature as a function of electric field for the two-flavor NJL model, showing the behavior previously predicted, that as we grow the electric field the pseudocritical temperature decreases until we reach a critical value $eE = 0.31$ GeV^2. At this point, the pseudocritical temperature starts increasing as we increase the electric field.

Next, we discuss our results for the SU(2) PNJL model. We show in Fig. 4 the expectation value of the Polyakov loop as a function of the temperature for different values of electric fields. We can see that the effect of the strong electric fields slightly changes the Polyakov loop expectation value in comparison with the effect on the effective quark mass. These changes are more prominent at $T \sim 170$ MeV, where the increase of the electric field tends to strengthen the deconfined phase. Also, we should mention that the effect of the electric field in the Polyakov loop is given in an indirect way though the gap equation (19) and Eq. (23) (that are coupled), once the electric fields do not couple directly with the Polyakov loop.

In Fig. 5 we show the effective quark masses as a function of the temperature for different values of electric fields in the two-flavor PNJL model; the behavior of M as a function of eE and T is in qualitative agreement with that predicted in the NJL model. The quantity $-\frac{dM}{dT}$ for the two-flavor PNJL model is in Fig. 6 and in Fig. 7 we show the pseudocritical temperature for the chiral symmetry restoration as a function of T, as we increase the electric field. The results obtained in the PNJL model are in quantitative

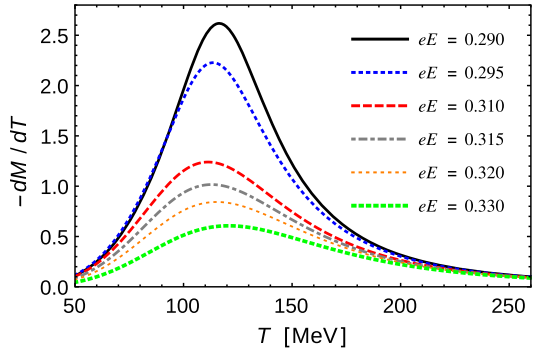

FIG. 2. Thermal susceptibility $-\frac{dM}{dT}$ as a function of the temperature for different values of eE in the SU(2) NJL model.

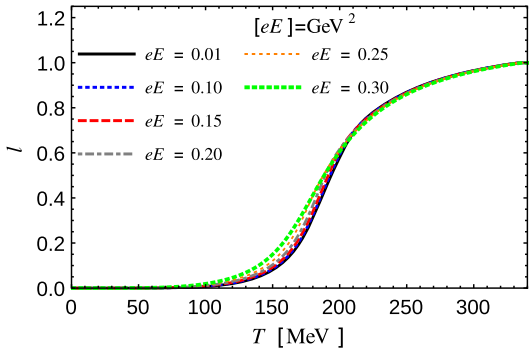

FIG. 4. Expectation value of the Polyakov loop for different values of eE in the PNJL model.

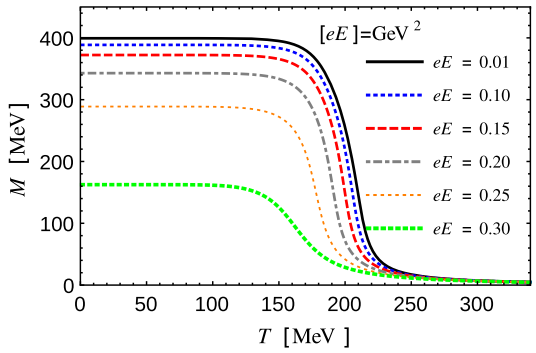

FIG. 5. Constituent quark mass as a function of T for different values of eE in the PNJL model.

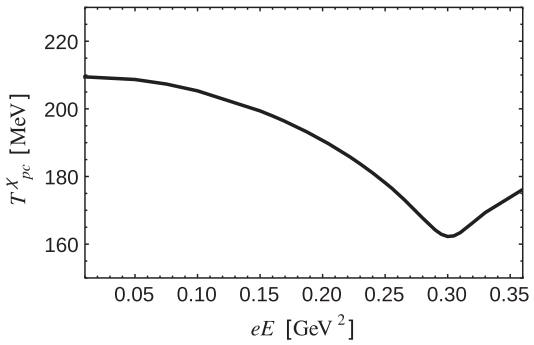

FIG. 7. Pseudocritical temperature T^{χ}_{pc} for chiral symmetry restoration of electrized quark matter as a function of the electric field eE in the PNJL model.

agreement with the NJL results, corroborating the idea that the present results are model independent.

The quantity $\frac{dl}{dT}$ as a function of the temperature for different values of electric fields is shown in Fig. 8; the pseudocritical temperature for deconfinement T^{l}_{pc} corresponds to the maximum of each curve for different values of electric fields. In Fig. 9 we show T^{l}_{pc} as a function of the electric field. The pseudocritical temperature for the deconfinement transition slightly decreases as we increase the electric field until $eE \sim 0.270$ GeV^2. At this point, the deconfinement temperature transition starts to increase in a similar way that we have predicted for the pseudocritical temperature for chiral symmetry restoration.

In Fig. 10 for the NJL SU(2) model the variation of the effective quark masses as a function of the electric field is shown for fixed temperatures: $T = 0$, 170, 200, and 220 MeV. At low values of the electric fields $eE \sim 0$, we can see the temperature effect on the partial restoration of the chiral symmetry. As we increase the magnitude of the electric field, the general aspect is the restoration of the chiral symmetry with the electric field.

For the PNJL SU(2) results we have almost the same analysis, but the quantitative results are different as we can see in Fig. 11. In Fig. 12, where we compare the two models at $T = 170$ MeV and $T = 220$ MeV, we can see quantitative differences on the numerical results.

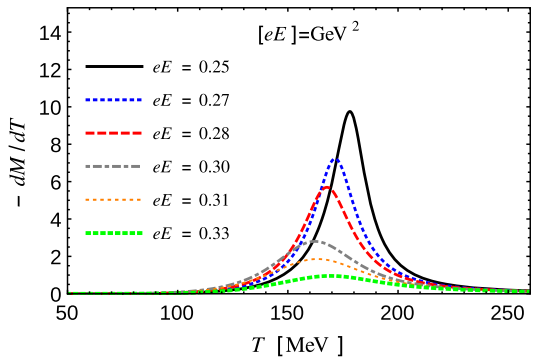

FIG. 6. $-\frac{dM}{dT}$ as functions of T for different values of eE in the PNJL model.

At $T = 170$ MeV the NJL SU(2) model partially restores the chiral symmetry with a lower electric field than the PNJL SU(2) model. In the lower panel of Fig. 12 we have the comparison of the models at $T = 200$ MeV. We see that the PNJL SU(2) model has a much higher value of the effective quark mass at $eE \sim 0$ than the NJL SU(2) model. Also, both models tends to partially restore the chiral symmetry to higher values of electric fields, following the previous analysis. At $T = 0$ almost no difference is seen. All these results show quantitative differences between the two models and how the confinement can change the scenario of the restoration of the chiral symmetry.

It is interesting to point out the prediction of the differences of the effects of the electric fields on T^{l}_{pc} and T^{χ}_{pc} in the PNJL model. The electric fields tends to influence more easily the chiral transition than the deconfinement. The behavior of the chiral condensate and the Polyakov loop in an environment with constant magnetic field has been explored in [31].

We see that the difference between the pseudocritical temperatures for chiral symmetry restoration at $eE = 0.15$ GeV^2 and $eE = 0.2$ GeV^2 is about $\Delta T^{\chi}_{pc} \sim 8.7$ MeV. In the same manner, the difference in the deconfinement temperature is given by $\Delta T^{l}_{pc} \sim 1.43$ MeV. As a conclusion, the quarks can be in a deconfined phase with chiral symmetry still not restored. This is a very interesting result, in the opposite direction of what happens when we have the

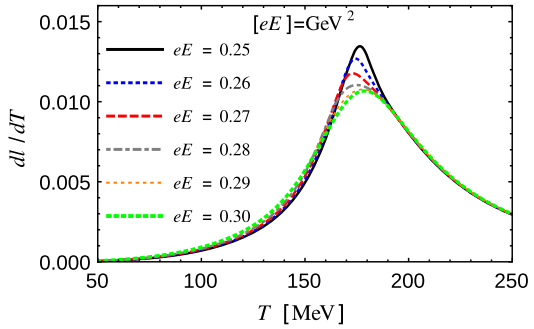

FIG. 8. $\frac{dl}{dT}$ as functions of T for different values of eE in the PNJL model.

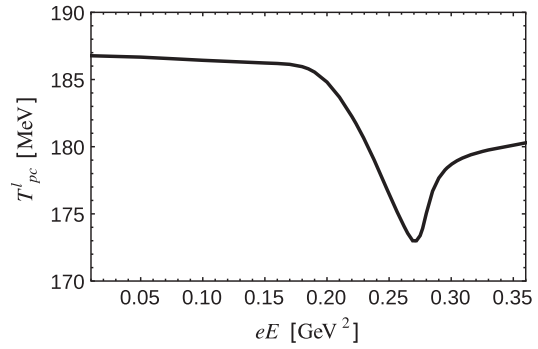

FIG. 9. The pseudocritical temperature T^{ϕ}_{pc} for the deconfinement transition of electrized quark matter as a function of the electric field eE in the PNJL model.

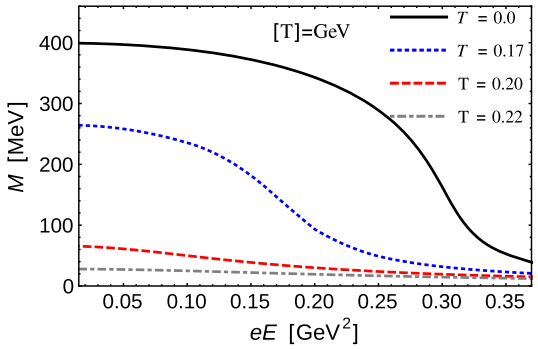

FIG. 10. Effective quark masses as a function of the electric field for fixed values of the temperature in the NJL SU(2) model.

quarkyonic phase [51,57] that occurs for some values of $\mu \neq 0$ and $eE = eB = 0$. At strong enough electric fields, where both T^{χ}_{pc} and T^{l}_{pc} increase as when we increase the electric field, the variation in the respective transition temperatures become larger and different. For example, if we take $eE = 0.25$ GeV^2 and $eE = 0.30$ GeV^2 we have, respectively, $\Delta T^{\chi}_{pc} \sim 15.88$ MeV and $\Delta T^{l}_{pc} \sim 2.18$ MeV. We should pay attention to the fact that we are working with magnitudes of the electrical fields that are valid for the NJL and PNJL models $eE \sim \Lambda^2$.

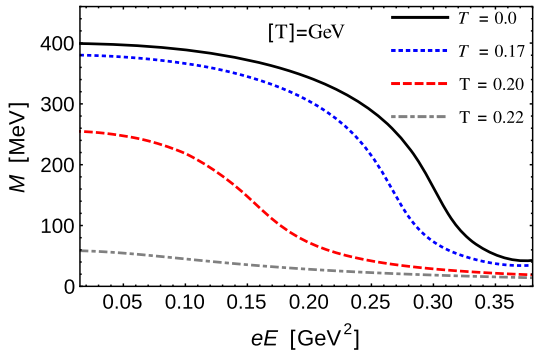

FIG. 11. Effective quark masses as a function of the electric field for fixed values of the temperature in the PNJL SU(2) model.

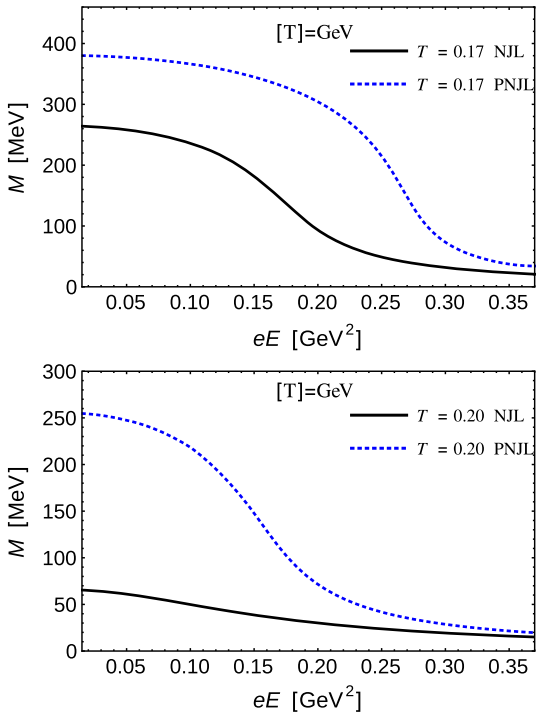

FIG. 12. Effective quark masses as a function of the electric field for fixed values of the temperature in the NJL SU(2) model compared with the PNJL SU(2) model for $T = 170$ MeV (top panel) and $T = 200$ MeV (bottom panel).

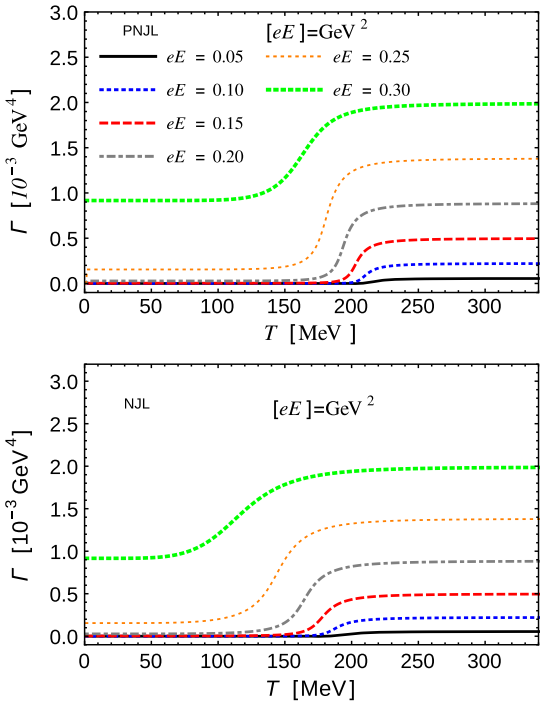

FIG. 13. Top: The pair production Γ of electrized quark matter as a function of the temperature for different values of electric fields in the PNJL model. Bottom: The same values of eE for the NJL model.

In Fig. 13 we show the Schwinger pair production as a function of the temperature at fixed electric fields $eE = 0.05\ \mathrm{GeV}^2$, $eE = 0.10\,\mathrm{GeV}^2$, $eE = 0.15\,\mathrm{GeV}^2$, $eE = 0.20\,\mathrm{GeV}^2$, $eE = 0.25\ \mathrm{GeV}^2$, and $eE = 0.30\ \mathrm{GeV}^2$. In the region where we have chiral symmetry restoration we can see that the production rate grows, and after some value of temperature the Schwinger pair production stabilizes. Another interesting aspect is that if you fix the electric field, in the NJL model the Schwinger pair production stabilizes for larger values and it happens at low temperatures if we compare with the PNJL model results.

V. CONCLUSIONS

In this work we have presented a study for strongly electrized quark matter within the SU(2) PNJL and NJL models at finite temperatures in the mean field approximation. We have shown that the constituent quark masses decrease as we grow both electric fields and temperatures, as a signature of the partial restoration of the chiral symmetry. In this scenario, as expected, the pseudocritical temperature for chiral symmetry restoration decreases as we grow the electric fields. The deconfinement is guided by the expectation value of the Polyakov loop, and our results show that the electric fields tend to anticipate the transition to the deconfined phase, and the effects due to the electric fields are more prominent in the chiral transition than the deconfinement one. On the other hand, we show that for strong enough electric fields, both pseudocritical temperatures for chiral symmetry and deconfinement temperatures start to increase after a critical value of the electric field, a very interesting effect that has been identified for the first time in the literature. This effect propagates to all quantities, as the Schwinger pair production. For comparison, we also show the results in the NJL model, where the same qualitative results are obtained, revealing that the main characteristics of this type of theory are model independent. Also, we observe that for some values of electric fields, the quarks can be in a deconfined phase with the chiral symmetry still not restored, in the opposite direction of the observed quarkyonic phase for systems at finite baryonic density and zero external fields. We expect to use this type of phenomenology to extend the analysis for electromagnetic fields and more general purposes in the future, e.g., in systems that present a chiral imbalance of right-handed and left-handed quarks, in finite baryonic densities, and in the physics behind the chiral magnetic effect [5,58,59]. Works in these directions are under way and we expect to report our results soon.

ACKNOWLEDGMENTS

This work is partially supported by Conselho Nacional de Desenvolvimento Científico e Tecnológico—CNPq, Grants No. 304758/2017-5 (R. L. S. F) and No. 6484/2016-1 (S. S. A); as part of the project Instituto Nacional de Ciência e Tecnologia—Física Nuclear e Aplicações (INCT-FNA) Grant No. 464898/2014-5 (S. S. A.); Fundação de Amparo à Pesquisa do Estado do Rio Grande do Sul (FAPERGS), Grant No. 19/2551-0000690-0 (R. L. S. F.); and Coordenação de Aperfeiçoamento de Pessoal de Nível Superior (CAPES) (W. R. T.), Brasil (CAPES), Finance Code 001.

APPENDIX: THE TRACE OF THE POLYAKOV LOOP

The Polyakov loop can be expressed by a diagonal matrix $L = \mathrm{diag}(e^{i\varphi}, e^{i\varphi'}, e^{-i(\varphi+\varphi')})$. As discussed in [42,60], the perturbative vacuum has $\varphi = \varphi' = 0$, i.e., the $T = 0$ limit, and the confining vacuum can be chosen to be $\varphi = \frac{2\pi}{3}$ and $\varphi' = 0$. For simplicity, we can adopt $\varphi' = 0$ from the beginning. The Polyakov loop with this assumption assumes $l = \frac{1}{N_c}\mathrm{Tr}_c L = \frac{1}{N_c}\mathrm{Tr}_c L^\dagger$. This is true for the limit $\mu = 0$ [61].

The simplification adopted here implies $l = \frac{1}{3}(1 + 2\cos\varphi)$. It is useful to invert the last relation for future evaluations:

$$\varphi = \cos^{-1}\left(\frac{3l-1}{2}\right). \tag{A1}$$

In this work we will implement the $\mu = 0$ case (where we have $\bar{l} = l$) and Tr_c; i.e., the trace over the color space is performed following the steps given in Eqs. (16) and (17). First we decompose the trace as

$$\mathrm{Tr}_c[(L)^n + (L^\dagger)^n] = \mathrm{Tr}_c(L)^n + \mathrm{Tr}_c(L^\dagger)^n. \tag{A2}$$

To evaluate the trace of L^n and $(L^\dagger)^n$ we should note that the *Ansatz* is already in the Jordan form [62]; then we can use the following result:

$$\mathrm{Tr}A^n = \sum_i \lambda_i^n, \tag{A3}$$

where the λ_i are the eigenvalues of the matrix A. Applying this result directly to Eq. (A2), we obtain

$$\begin{aligned}\mathrm{Tr}_c(L)^n + \mathrm{Tr}_c(L^\dagger)^n &= 2(1 + e^{i\varphi n} + e^{-i\varphi n}),\\ &= 2(1 + 2\cos n\varphi).\end{aligned} \tag{A4}$$

Using now Eq. (A1) in the last equation, we can reach

$$\begin{aligned}&\mathrm{Tr}_c(L)^n + \mathrm{Tr}_c(L^\dagger)^n\\ &\quad= 2 \times \left\{1 + 2\cos\left[n\cos^{-1}\left(\frac{3l-1}{2}\right)\right]\right\}.\end{aligned} \tag{A5}$$

[1] A. Bzdak and V. Skokov, Phys. Lett. B **710**, 171 (2012).
[2] W. T. Deng and X. G. Huang, Phys. Rev. C **85**, 044907 (2012).
[3] J. Bloczynski, X. G. Huang, X. Zhang, and J. Liao, Phys. Lett. B **718**, 1529 (2013).
[4] W. T. Deng and X. G. Huang, Phys. Lett. B **742**, 296 (2015).
[5] K. Fukushima, D. E. Kharzeev, and H. J. Warringa, Phys. Rev. D **78**, 074033 (2008); D. E. Kharzeev and H. J. Warringa, Phys. Rev. D **80**, 034028 (2009); D. E. Kharzeev, Nucl. Phys. **A830**, 543c (2009).
[6] R. Duncan and C. Thompson, Astron. J. **392**, L9 (1992).
[7] C. Kouveliotou *et al.*, Nature (London) **393**, 235 (1998).
[8] J. Bloczynski, X. G. Huang, X. Zhang, and J. Liao, Nucl. Phys. **A939**, 85 (2015).
[9] Y. Hirono, M. Hongo, and T. Hirano, Phys. Rev. C **90**, 021903(R) (2014).
[10] V. Voronyuk, V. D. Toneev, S. A. Voloshin, and W. Cassing, Phys. Rev. C **90**, 064903 (2014).
[11] Y.-L. Cheng, S. Zhang, Y.-G. Ma, J.-H. Chen, and C. Zhong, Phys. Rev. C **99**, 054906 (2019).
[12] H. Li, X.-l. Sheng, and Q. Wang, Phys. Rev. C **94**, 044903 (2016).
[13] J. Zhao and F. Wang, Prog. Part. Nucl. Phys. **107**, 200 (2019).
[14] X. G. Huang and J. Liao, Phys. Rev. Lett. **110**, 232302 (2013).
[15] Y. Jiang, X. G. Huang, and J. Liao, Phys. Rev. D **91**, 045001 (2015).
[16] S. Pu, S.-Y. Wu, and D.-L. Yang, Phys. Rev. D **91**, 025011 (2015).
[17] S. Pu, S.-Y. Wu, and D.-L. Yang, Phys. Rev. D **89**, 085024 (2014).
[18] X. G. Huang, Rep. Prog. Phys. **79**, 076302 (2016).
[19] V. A. Miransky and I. A. Shovkovy, Phys. Rep. **576**, 1 (2015); D. Ebert, K. G. Klimenko, M. A. Vdovichenko, and A. S. Vshivtsev, Phys. Rev. D **61**, 025005 (1999); K. G. Klimenko, Z. Phys. C **54**, 323 (1992); arXiv:hep-ph/9809218.
[20] D. P. Menezes, M. Benghi Pinto, S. S. Avancini, and C. Providência, Phys. Rev. C **80**, 065805 (2009).
[21] D. P. Menezes, M. Benghi Pinto, S. S. Avancini, A. Pérez Martínez, and C. Providência, Phys. Rev. C **79**, 035807 (2009).
[22] R. L. S. Farias, K. P. Gomes, G. I. Krein, and M. B. Pinto, Phys. Rev. C **90**, 025203 (2014).
[23] R. L. S. Farias, V. S. Timoteo, S. S. Avancini, M. B. Pinto, and G. Krein, Eur. Phys. J. A **53**, 101 (2017).
[24] S. S. Avancini, R. L. S. Farias, M. Benghi Pinto, W. R. Tavares, and V. S. Timóteo, Phys. Lett. B **767**, 247 (2017).
[25] S. S. Avancini, R. L. S. Farias, and W. R. Tavares, Phys. Rev. D **99**, 056009 (2019).
[26] A. Ayala, M. Loewe, A. Z. Mizher, and R. Zamora, Phys. Rev.D **90**, 036001 (2014).
[27] A. Ayala, M. Loewe, and R. Zamora, Phys. Rev. D **91**, 016002 (2015).
[28] G. S. Bali, F. Bruckmann, G. Endrődi, Z. Fodor, S. D. Katz, S. Krieg, A. Schäfer, and K. K. Szabó, J. High Energy Phys. 02 (2012) 044.
[29] G. S. Bali, F. Bruckmann, G. Endrődi, Z. Fodor, S. D. Katz, and A. Schäfer, Phys. Rev. D **86**, 071502(R) (2012).
[30] K. Fukushima and T. Hatsuda, Rep. Prog. Phys. **74**, 014001 (2011).
[31] K. Fukushima, M. Ruggieri, and R. Gatto, Phys. Rev. D **81**, 114031 (2010).
[32] R. Gatto and M. Ruggieri, Phys. Rev. D **82**, 054027 (2010).
[33] R. Gatto and M. Ruggieri, Phys. Rev. D **83**, 034016 (2011).
[34] K. Kashiwa, Phys. Rev. D **83**, 117901 (2011).
[35] G. Endrődi and G. J. Marko, J. High Energy Phys. 08 (2019) 036.
[36] L. D Mclerran and B. Svetitsky, Phys. Rev. D **24**, 450 (1981).
[37] M. Cheng *et al.*, Phys. Rev. D **77**, 014511 (2008).
[38] C. Ratti, S. Rőssner, M. Thaler, and W. Weise, Eur. Phys. J. C **49**, 213 (2007).
[39] C. Ratti, M. A. Thaler, and W. Weise, Phys. Rev. D **73**, 014019 (2006).
[40] K. Fukushima and C. Sasaki, Prog. Part. Nucl. Phys. **72**, 99 (2013).
[41] H. Hansen, W. M. Alberico, A. Beraudo, A. Molinari, M. Nardi, and C. Ratti, Phys. Rev. D **75**, 065004 (2007).
[42] J. O. Andersen, W. R. Naylor, and A. Tranberg, Rev. Mod. Phys. **88**, 025001 (2016).
[43] Y. Nambu and G. Jona-Lasinio, Phys. Rev. **122**, 345 (1961); **124**, 246 (1961).
[44] W. R. Tavares and S. S. Avancini, Phys. Rev. D **97**, 094001 (2018).
[45] G. Cao and X. G. Huang, Phys. Rev. D **93**, 016007 (2016).
[46] M. Ruggieri, Z. Y. Lu, and G. X. Peng, Phys. Rev. D **94**, 116003 (2016).
[47] M. Ruggieri and G. X. Peng, Phys. Rev. D **93**, 094021 (2016).
[48] J. S. Schwinger, Phys. Rev. **82**, 664 (1951).
[49] W. Heisenberg and H. Euler, Z. Phys. **98**, 714 (1936).
[50] K. Fukushima, Phys. Rev. D **77**, 114028 (2008).
[51] J. P. Carlomagno and M. Loewe, Phys. Rev. D **95**, 036003 (2017).
[52] S. P. Klevansky, Rev. Mod. Phys. **64**, 649 (1992); S. P. Klevansky and R. H. Lemmer, Phys. Rev. D **39**, 3478 (1989).
[53] M. Buballa, Phys. Rep. **407**, 205 (2005).
[54] A. Ayala, C. A Dominguez, L. A. Hernandez, M. Loewe, A. Raya, J. C. Rojas, and C. Villavicencio, Phys. Rev. D **94**, 054019 (2016).
[55] B.-J. Schaefer, J. M. Pawlowski, and J. Wambach, Phys. Rev. D **76**, 074023 (2007).
[56] H. Suganuma and T. Tatsumi, Prog. Theor. Phys. **90**, 379 (1993).
[57] L. McLerran, K. Redlich, and C. Sasaki, Nucl. Phys. **A824**, 86 (2009).
[58] R. L. S. Farias, D. C. Duarte, G. Krein, and R. O. Ramos, Phys. Rev. D **94**, 074011 (2016).
[59] D. E. Kharzeev, L. D. McLerran, and H. J. Warringa, Nucl. Phys. **A803**, 227 (2008).
[60] K. Fukushima, Phys. Lett. B **591**, 277 (2004).
[61] H. Abuki and K. Fukushima, Phys. Lett. B **676**, 57 (2009).
[62] A. R. Horn and C. R. Johnson, *Matrix Analysis*, 2nd ed. (Cambridge University Press, New York, 2013).